IAC–24–A2,3,11,x85867

Parameter Identification using Microgravity Experiments in Asteroid-related Scenarios

Samuele Vaghi[a*], Alessia Cremasco[b], Luigi Vittorio Delfanti[c], Iosto Fodde[d], Fabio Ferrari[e]

[a] *Department of Aerospace Science and Technology, Politecnico di Milano, Via La Masa 34, Milano, Italy, samuele.vaghi@polimi.it*
[b] *alessia.cremasco@polimi.it,*
[c] *luigivittorio.delfanti@mail.polimi.it,*
[d] *iosto.fodde@polimi.it,*
[e] *fabio1.ferrari@polimi.it,*
[*] *Corresponding author*

Abstract

The increasing interest in asteroid science and explorations calls for the need of accurate dynamical models. Most asteroids are now thought to be rubble-piles, i.e. aggregates of material held together by cohesion and gravitational forces rather than their bulk material's strength. They can be effectively modelled in numerical simulations using N-body codes such as GRAINS, whose contact dynamics is based on Project Chrono. This research aims at filling the gap in the validation of contact models, whose parameters are generally tuned to reproduce large-scale behaviour rather than the local-scale interactions. To this aim, a microgravity and vacuum experiment is under development. The high-level goal is to observe the collision of two centimeters-sized asteroid simulant cobbles. A digital twin of the experiment, created in GRAINS, will be used to reproduce the outcomes of the experiment, tuning the contact parameters that to obtain the best fit with the experimental data. This paper presents the preliminary activities aimed at testing each component of the experimental setup in preparation for the actual campaign.

Acronyms

C::E	Project Chrono.
CoM	Center of Mass.
CoR	Coefficient of Restitution.
DEM	Discrete Element Method.
EPM	Electropermanent Magnet.
FoV	Field of View.
FPS	Frames per second.
IMU	Inertial Measurement Unit.
NSC	Non-Smooth Contacts.
PCC	Phantom Camera Control.
SMC	SMooth Contacts.

1. Introduction

The field of small Solar System bodies research and exploration is experiencing an unprecedented growth. This can be attributed to three main reasons: their scientific relevance, the potential for resource utilization, and concerns related to planetary defense [1]. There is evidence, based on the study of their rotational period, that most asteroids with characteristic dimension between $100\ m$ and $100\ km$ are gravitational aggregates rather than monolithic bodies [2]. This finding is further supported by in-situ measurements performed by asteroid exploration missions, such as Hayabusa at Itokawa [3], Hayabusa2 at Ryugu [4], OSIRIS-REx at Bennu [5], and DART at Dimorphos [6]. These considerations imply that such gravitational aggregates, referred to as rubble-piles, should be treated as granular systems, with dynamics that are complex to model, either analytically or numerically. The dynamics of a rubble-pile asteroid lead to a gravitational-collision problem that, in the low-energy regime, can be numerically solved using N-body codes. These simulations rely on the Discrete Element Method (DEM) to introduce contact interactions between each particle. The methods implemented are classified into two categories: soft-body and hard-body methods. In soft-body methods, colliding bodies are allowed to experience a small overlap, and the contact force is modeled through a spring-dashpot system. On the other hand, hard-body methods enforce a non-penetration condition between the bodies, with the contact force introduced as an impulsive force. Both methods have been applied to scenarios of interest in the literature [7] [8].

In particular, the N-body code GRAINS is capable of simulating interactions between irregularly-shaped particles [9] [10], which is essential for enhancing the realism of

the simulations. Its contact dynamics are based on the physics engine Project Chrono (C::E) [11]. Relevant parameters for soft and hard body models include include the coefficient of friction (static, dynamic, spinning), cohesion (modelled as an attractive force at contact points), stiffness, and damping. Using either method, all these parameters shall be tuned. This is generally done to fit at best the macroscopic behaviour of the system. However, a code whose contact dynamics are validated to reliably represent the interactions at particle-scale is expected to enhance the realism of the simulations.

To this end, an experimental campaign is under development. The goal is to leverage on the advanced capabilities of C::E to simulate contact dynamics, and validate it for asteroid-related scenarios. The high-level objective of the experiment is to observe the collision of asteroid simulant cobbles in vacuum and microgravity conditions, which are necessary to replicate the asteroid environment. Then, the data collected will be used to calibrate the relevant contact parameters in C::E.

The paper is organized as follows: in Section 2 the numerical model used as a benchmark for the experiment is described, then in Section 3 the general experimental setup is presented, addressing each component. In Section 4 the results relative to the preliminary tests are presented; eventually, in Section 5 concluding remarks are provided.

2. Dynamics

The main objective of the experiment is to characterize particle-scale interactions in a vacuum and microgravity asteroid simulation environment. Subsequently, the results of the experiment will be exploited to validate numerical simulations in N-body programs, such GRAINS, and to calibrate contact methods and parameters. This Section describes the numerical model developed in GRAINS to validate the methodology.

The asteroid-simulant cobbles are modelled as three-dimensional rigid bodies with 6 degrees of freedom. Their state vector $\boldsymbol{x}$ includes the position and velocity of their Center of Mass (CoM), $\boldsymbol{r}_{CoM}$ and $\boldsymbol{v}_{CoM}$ respectively, the quaternion $\boldsymbol{q}$ indicating the attitude of the body's principal axis frame with respect to the inertial frame, and the angular velocity ${}^{B}\boldsymbol{\omega}$ expressed in the body frame. Hence, $\boldsymbol{x} = [\boldsymbol{r}_{CoM}, \boldsymbol{v}_{CoM}, \boldsymbol{q}, {}^{B}\boldsymbol{\omega}]^T$.

As compromise between realism and computational effort of the simulation, preliminary numerical tests are performed using the shape model of asteroid Bennu (based on radar observations [12]) to create the two colliding bodies. This model has been scaled and slightly modified to replicate characteristics that are comparable to those of the cobbles (detailed in Subsection 3.4). The resulting inertial properties and dimensions are reported in Table 1.

Table 1. Properties of colliding bodies in the simulation.

Mass $[kg]$	Characteristic length $[m]$	Inertia tensor $[kg/m^2]$	Number of vertices
1.1571	0.1188	diag([0.001119, 0.001010, 0.000817])	1348

A collision scenario consistent with the predicted experiment result has been developed in GRAINS.

As mentioned, there are several approaches to solve the contact interaction between particles in DEM simulations. Within C::E, the following contact models are implemented: *smooth contacts*, *non-smooth contacts*, and *non-smooth contacts with compliance*. The SMooth Contacts (SMC) is a force-based soft-body method [13], with relevant parameters including coefficients of friction (static, dynamic, spinning), cohesion, stiffness, and damping. In contrast, the Non-Smooth Contacts (NSC) is an impulse-based hard-body method [14]. While it shares key parameters with SMC (coefficients of friction and cohesion), the contact interactions are defined by the Coefficient of Restitution (CoR). Additionally, a third model implemented in C::E introduces compliance and damping in non-smooth contacts [15].

The NSC with compliance is selected as the most suitable approach for replicating the experiment due to its versatility. While the collision between the two bodies is expected to behave as nearly rigid, this method also allows for the inclusion of cohesion forces, which are crucial in full-scale asteroid evolution problems. Nevertheless, each contact model will be compared with experimental data for further investigations.

Snapshots from the benchmark simulation are shown in Fig. 1, illustrating the state of the simulation at the beginning, right before the collision, and at the end (after 2.5 seconds).

The selected values for some relevant parameters are reported in Table 2.

The initial conditions are set as follows: inclination angle $\alpha = 60°$, initial velocity magnitude $\|\boldsymbol{v}_0\| = 0.26$ m/s, zero initial angular velocity, and initial position $\boldsymbol{r}_0$ and quaternion $\boldsymbol{q}_0$ as reported in Table 3.

Table 2. NSC parameters of the simulation.

CoR [-]	Static Friction [-]	Compliance $[m/N]$
0.6	0.8	1e-4

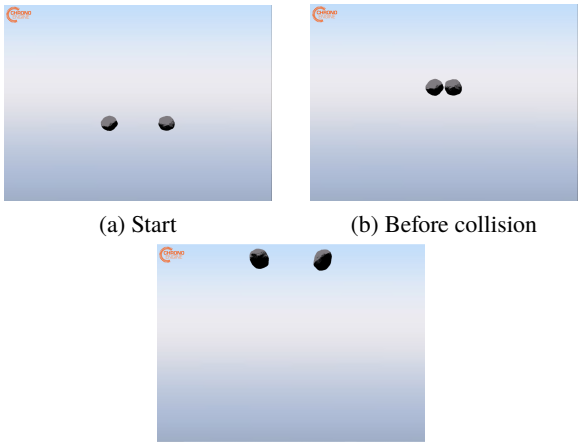

(a) Start (b) Before collision

(c) End

Fig. 1. Simulation snapshots.

Table 3. Initial position and quaternion of bodies in the simulation.

Body	$\boldsymbol{r}_0$ [m]	$\boldsymbol{q}_0$ [-]
Body 1	$[-0.153, 0.08, 0]^T$	$[0.600, 0.000, 0.000, -0.800]^T$
Body 2	$[0.153, 0.08, 0]^T$	$[0.600, 0.000, 0.000, 0.800]^T$

In the real experiment, a high-fidelity model incorporating the 3D mesh and measured inertial properties of the specific cobbles will be fed to the numerical solver to enhance the realism of the simulation. A 3D scanner has been used for this purpose.

3. Experimental set-up

A scheme of the validation campaign logic is reported in Fig. 2.

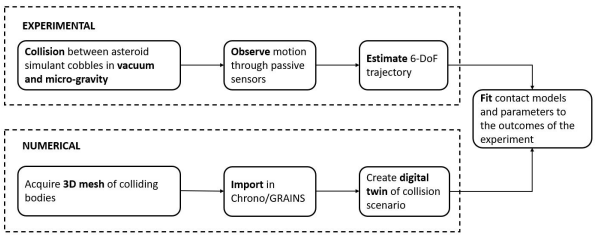

Fig. 2. Experiment Layout.

In the following sections, the requirements and solutions identified for each component of the experiment are discussed.

3.1 Drop Tower Facility

The typical gravitational acceleration found on hundreds-meter sized asteroids is in the order of $10^{-6} - 10^{-5} g_0$ [16], meaning that similar levels of acceleration shall be achieved to reproduce with high fidelity the asteroid environment. This is possible in the ZARM Drop Tower, located in Bremen [17]. In order to minimize disturbances, air is pumped out from the tower and a capsule, containing the experiment, is dropped from the top. The free fall lasts about 5 seconds. Sensors and a data acquisition system are embedded in the capsule as well. In case vacuum conditions are necessary, it is possible to mount a vacuum chamber within the capsule. For this purpose, the vacuum chamber developed by JAXA and used in drop tower tests in preparation to Hayabusa2 mission will be used. The drop tower and capsule layout is reported in Fig. 3.

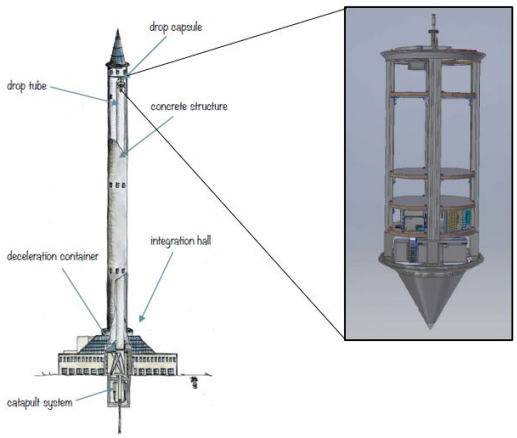

Fig. 3. Drop Tower Layout [17].

3.2 Cameras

The choice of the sensors is driven by the need to minimize the interaction with the free-motion of the cobbles. For this reason, it has been chosen to use high-speed, high-resolution cameras. The cameras are also required to withstand the deceleration occurring at the end of the drop, that is in the order of 50-g. A set of Phantom Miro C321 cameras will be provided by ZARM, but they can only be placed outside of the vacuum chamber. In order to obtain optical measurements from more perspectives, two additional cameras will be placed inside the vacuum chamber. Among commercial cameras, GoPros represent the best compromise between the achievable resolution, frame rate and high-g resistance. The specifications of the cameras can be found in Table 4.

Once the video is acquired, a set of markers placed on the cobbles will be tracked using the Phantom Camera Con-

Table 4. Camera Data.

Model	FPS	Resolution [px]	FoV [deg]
Phantom C321	1480	1920×1080	70×56
GoPro 12	240	2704×1520	87×56

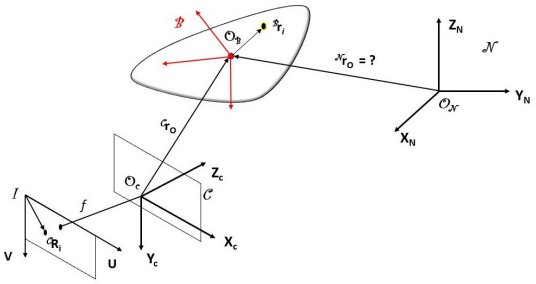

Fig. 4. Reference Frames. $\mathcal{N}$ is the inertial reference frame, $\mathcal{B}$ is the body reference frame, $\mathcal{C}$ is the camera reference frame, and I is the image plane.

trol (PCC) software. Hence, the available measurements are the 2D pixel coordinates in camera frame.

3.3 Estimation Algorithm

An estimation strategy is necessary to estimate the cobbles' trajectory, which will be used, in turn, as reference trajectory in the numerical solver. The discontinuity introduced by the collision represents a challenge for the estimation algorithm. Hence, the estimation will be split in two arcs: before and after the collision. The variables characterizing the collision, such as energy and CoR, will be recovered afterwards, as done in previous asteroid-related drop tower experiments [18]. Due to its reliability and simplicity, a least-squares batch filter is used to estimate the initial state of the cobbles on each arc. The approach implemented is inspired by vision-based navigation techniques [19] [20]. Starting from an initial guess for each state variable (i.e. position, velocity, attitude and angular velocity), the dynamics are propagated along each arc, and the position of each marker in world coordinates is projected onto the 2D camera frame (see Fig. 4). Then, the residuals (i.e. the difference between the measured pixel coordinates and the projected ones), are used to build the cost function that will be minimized in the filter. The accurate knowledge of the position of each marker in the body frame is key to the success of the estimation procedure. For this reason, the shape model acquired for each cobble is also used to set the position of the markers in body frame.

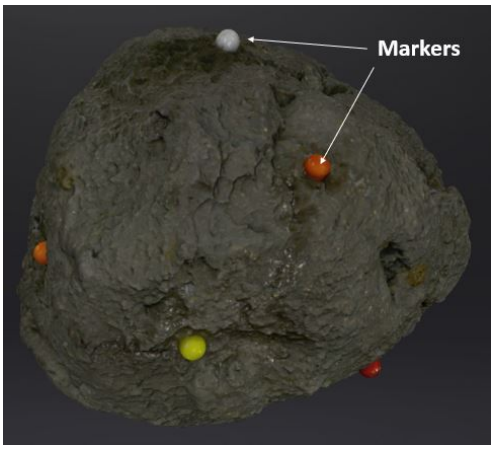

Fig. 5. Scanned shape of a CIE simulant.

3.4 Simulant Material

Some requirements have been considered to select the cobbles:

- Chemical composition: it shall resemble as closely as possible the one of asteroid material;
- Surface properties: as no atmosphere is present on asteroids, the cobbles shall not be bevelled by weathering;
- Dimensions: shall be compatible with the internal dimensions of the vacuum chamber. Ideal cobbles size has been chosen between 8 and 10 cm.

A set of cobbles has been purchased from Space Resource Technologies, a laboratory specialized in the production of regolith and asteroid simulants. The chemical composition of their simulants is based on the one of meteorites found on the Earth [21]. Hence, it is ideal to fulfill the first requirement. The cobbles are classified depending on which meteroite they are based on. For this work, simulants based on the Orgueil and Murchison meteorite have been chosen. They are classified respectively as CIE and CME [21]. However, it was necessary to have more spare material for preliminary tests. Therefore, a third set of cobbles has been sampled on Mount Etna: coming from recent volcanic eruptions, they meet the second requirement.
Markers have been glued to the surface of each cobble: an example is visible in Fig. 5. As previously anticipated, the 3D scan of each of them has been acquired in order to generate a 3D mesh and to recover inertia properties and markers' positions, fundamental for the estimation algorithm.
It is also interesting to investigate the density distribution

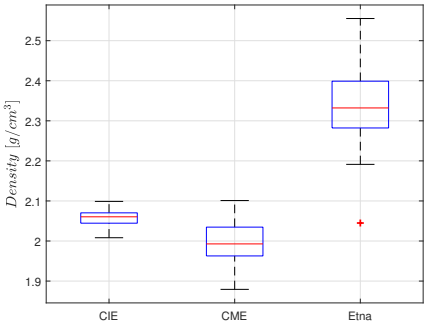

Fig. 6. Simulants density distribution.

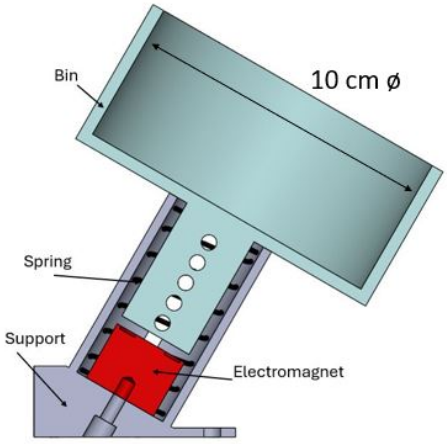

Fig. 7. Release Mechanism.

of the cobbles, obtained by weighting the cobbles and computing their volume from the shape model. Fig. 6 reports the density recovered for Etna, CME and CIE rocks. The latter are more lightweight and present a smaller standard deviation with respect to Etna rocks. This outcome was expected: indeed, CIE and CME simulants are artificial cobbles, prepared following a specific procedure, whereas Etna rocks have been sampled in nature. Moreover, there may be inclusions of magma that solidified at different stages, causing small fluctuations in the bulk density of the rocks.

3.5 Release Mechanism

A release mechanism is necessary to push the cobbles against each other and make the collision possible. A spring-based mechanism is considered. Two compression springs will be initially compressed thanks to an Electropermanent Magnet (EPM). After the capsule is dropped from the top of the tower, the EPM is activated and the springs are free to elongate and push the baskets that accommodate the cobbles. A cross-view of the CAD model is shown in Fig. 7 to support the explanation.

The Capsule Control System at ZARM allows to control the activation of the EPM. However, to test the mechanism in the lab, a RaspberryPi microcontroller has been used, in combination with an STM-Nucleo solid-state relay, necessary to dela with the 24VDC voltage required by the EPM.
In order to assess the repeatability of the release mechanism, an Inertial Measurement Unit (IMU) is launched inside a test body. The acceleration is integrated across the ejection time-window, thus recovering the velocity profile. Fig. 8 shows that the release mechanism provides similar performances in all the cases tested.

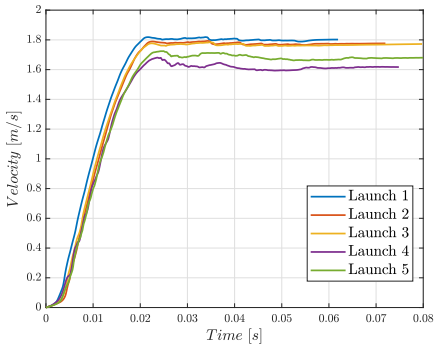

Fig. 8. Release Velocity Profile.

The flat region in the velocity profile corresponds to the time during which the object was in flight. Hence, the IMU can not measure any acceleration and the velocity remains constant.
Note that the springs used for preparatory tests are different from the ones that will be used in microgravity conditions. Indeed, in order to obtain an adequate release and

trajectory in ground tests, the gravity force shall be taken into account. The features of the two springs can be found in Table 5, where L is the length, D_{int} is the internal diameter, and K_{el} is the spring constant.

Table 5. Spring Data.

Model	L [mm]	D_{int} [mm]	K_{el} [N/mm]
Ground	60	26	2
Microgravity	60	26	0.2

4. Lab tests

A mock-up of the experimental setup has been developed, with the purpose of testing the procedure in preparation for the real experiment. Fig. 9 shows the mock-up, with two GoPros recording from the external view-ports. The two release mechanisms are screwed to an integration plate, mounted inside the chamber.

Fig. 9. Mock-up of the experimental setup.

4.1 Camera Calibration

To use cameras as sensors, the cameras shall be calibrated. Camera calibration is the procedure through which the intrinsic and extrinsic camera parameters are estimated [22]. Extrinsic parameters consist in the relative roto-translation between the optical center of the camera and the reference coordinate frame, whereas the intrinsic ones are necessary to transform the 3D coordinates in camera frame into 2D coordinates. The procedure followed for calibration is the checkerboard method, through the Camera Calibrator application in Matlab. It is based on the algorithm in [23]. The calibration pattern is left in the chamber to serve as a fixed reference frame for the estimation.

Stereo Camera Calibration In case more than one camera is used, the fixed pattern may not in the field of view of one of the cameras. This is often the case when a camera is placed inside the chamber. Hence, stereo camera calibration can be exploited to recover not only the parameters of each single camera, but also the relative roto-translation between the two. The method used is similar to the one used for single camera calibration. The dimensional limitations become crucial, since the same pattern shall be visible from both cameras. Moreover, the two cameras shall be synchronized as accurately as possible. This is done thanks to a LED light in view for both cameras.

4.2 Launches

In preparation to the experimental campaign, several launches have been performed, with increasing level of realism. The results relative to two of them are presented here, in order to show the performances of the proposed estimation strategy.

Launch 1 This test case has been performed launching only one rock. One camera is placed in the lower-left viewport, whereas the second one is placed inside the vacuum chamber. For the sake of simplicity, they will be referred to as Camera A and Camera B in the following. Once the initial state is estimated, the trajectory can be propagated forward in time, and the markers' positions can be projected back to camera plane to check the results. Fig. 10 and Fig. 11 show that a good correspondence between the estimated markers' trajectories and the actual measurements has been achieved.

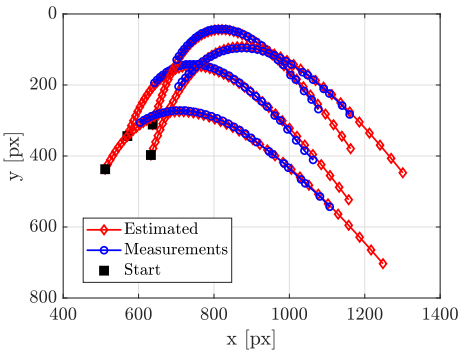

Fig. 10. Camera A: comparison between the measured and estimated trajectories of markers.

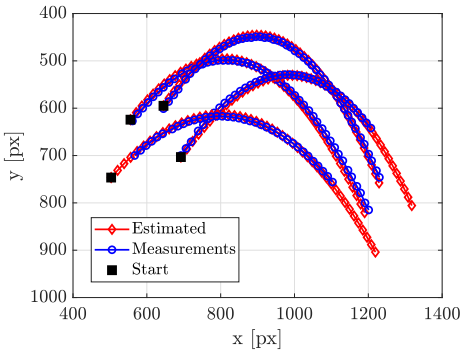

Fig. 11. Camera B: comparison between the measured and estimated trajectories of markers.

This can also be assessed by observing the trend of the post-estimation residuals, reported in Fig. 12.

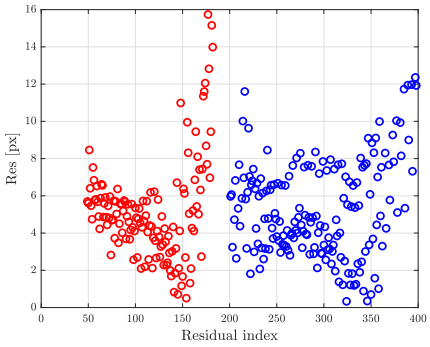

Fig. 12. Launch 1 - Residuals trend. In red, residuals from Camera A, in blue, residuals from Camera B.

The average residual recovered is $5.24\ px$. Each marker is $4\ mm$ wide, which corresponds to a size of approximately $10 - 15\ px$ when projected onto the image plane. Therefore, the average post-fit residual value obtained can be considered acceptable.
A further validation can be done exploiting triangulation. Indeed, for stereo-calibrated camera pairs, it is possible to reconstruct the 3D location of points detected in the 2D image plane of each camera [22]. Hence, the triangulated markers' positions can be compared to the ones recovered through the previously presented estimation algorithm: they are reported in Fig. 13.

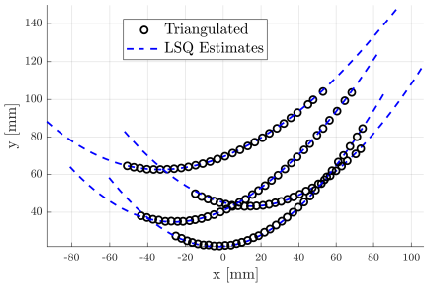

Fig. 13. Launch 1 - Comparison between triangulated and estimated markers' position

The norm of the error between estimated and triangulated points is shown in Fig. 14.

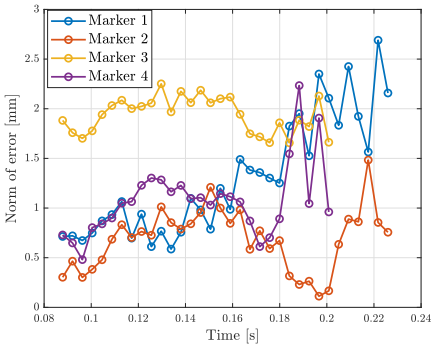

Fig. 14. Launch 1 - Error norm between triangulated points and trajectory estimated through least-squares batch filter.

Since the maximum error is lower than $2.5\ mm$, it is possible to state that the estimation algorithm provided satisfactory results.

Launch 2 Here we present the results relative to a launch performed with the two GoPros recording from

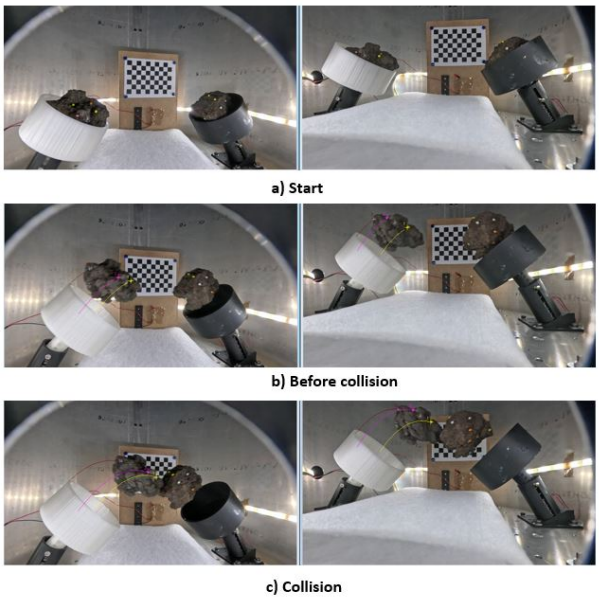

Fig. 15. Experiment snapshots

the outer view-ports, specifically the lower-left and lower-right ones (as in Fig. 9), and with the two rocks colliding. Snapshots from the recordings are provided in Fig. 15.

As done for the previous example, the re-projected markers' coordinates, relative to the rock on the left in Fig. 15, are compared to the measurements in Fig. 16 and Fig. 17. The post-fit residuals are reported as well (Fig. 18).

Also in this case, triangulation has been applied to check

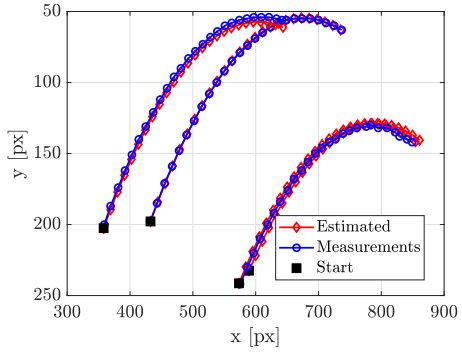

Fig. 16. Launch 2 - Camera A: comparison between the measured and estimated trajectories of markers.

the results. They are shown in Fig. 19 and Fig. 20.

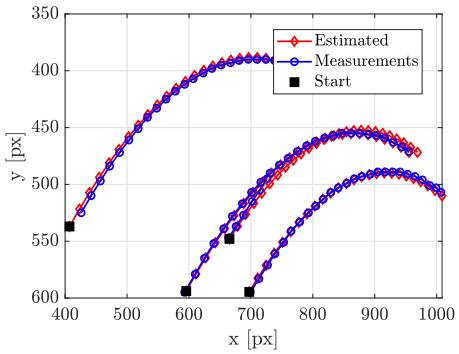

Fig. 17. Launch 2 - Camera B: comparison between the measured and estimated trajectories of markers.

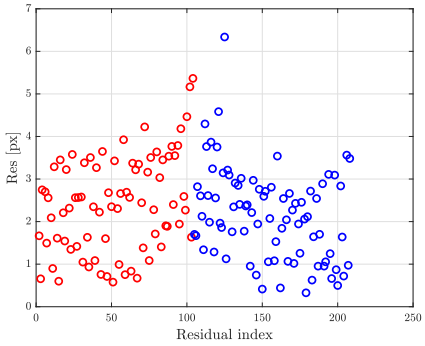

Fig. 18. Launch 2 - Residuals trend. In red, residuals from Camera A, in blue, residuals from Camera B.

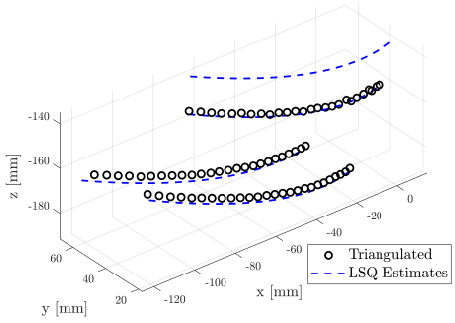

Fig. 19. Launch 2 - Comparison between triangulated and estimated markers' position.

Note that in this experiment, for one of the tracked markers, it was impossible to apply triangulation, since the marker was never visible from both cameras at the same time. This consideration points out the advantage of using directly the 2D pixel coordinates as measurements.

Indeed, the estimation works also in case a marker is visible from only one camera, as the 3D information come from the scan model. The norm of the error between estimated and triangulated points is shown in Fig. 20: the maximum error is lower than 3.5 mm.

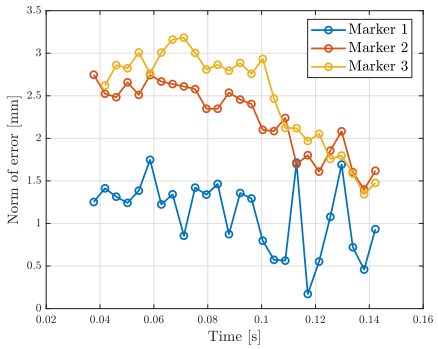

Fig. 20. Launch 2 - Error norm between triangulated points and trajectory estimated through least-squares batch filter.

5. Conclusions

In this paper, the activities performed in preparation to an experimental campaign aimed at investigating the particle-scale contact dynamics between asteroid simulant cobbles in vacuum and microgravity conditions are presented. The campaign will take place at ZARM Drop Tower, in Bremen, in November 2024. The development of the main components of the experimental setup is presented and discussed.

The release mechanism proved reliable in all the cases tested. Concerning the simulant material, the cobbles are either suited to represent the chemical composition of known meteorites or to reproduce the non-weathered surface that can be expected for asteroid material. Density distributions in agreement with the expectations have been recovered.

The results presented are relative to tests performed in the lab, aimed at reproducing the real experimental setup as realistically as possible. They show that the tracking and estimation procedures necessary to achieve the experiment's goals provide good performances. A general digital twin of the experiment has already been created in GRAINS, so that, after the campaign will be carried out, the data obtained will be analyzed and fed to the multibody solver in order to validate the contact dynamics algorithms.

Acknowledgements

Funded by the European Union (ERC, TRACES, 101077758). Views and opinions expressed are however those of the authors only and do not necessarily reflect those of the European Union or the European Research Council. Neither the European Union nor the granting authority can be held responsible for them.

References

[1] V. Badescu, *Asteroids: Prospective Energy and Material Resources*. 2013.

[2] D. C. Richardson, Z. M. Leinhardt, H. Melosh, W. Bottke Jr, E. Asphaug, *et al.*, "Gravitational aggregates: Evidence and evolution," *Asteroids iii*, vol. 1, pp. 501–515, 2002.

[3] A. Fujiwara *et al.*, "The rubble-pile asteroid Itokawa as observed by hayabusa," *Science*, vol. 312, no. 5778, pp. 1330–1334, 2006.

[4] S. Watanabe *et al.*, "Hayabusa2 arrives at the carbonaceous asteroid 162173 Ryugu—a spinning top–shaped rubble pile," *Science*, vol. 364, no. 6437, pp. 268–272, 2019.

[5] O. Barnouin *et al.*, "Shape of (101955) Bennu indicative of a rubble pile with internal stiffness," *Nature geoscience*, vol. 12, no. 4, pp. 247–252, 2019.

[6] S. Raducan *et al.*, "Physical properties of asteroid dimorphos as derived from the dart impact," *Nature Astronomy*, vol. 8, no. 4, pp. 445–455, 2024.

[7] D. J. Sánchez; Scheeres, "Simulating asteroid rubble piles with a self-gravitating spft-sphere distinct element method model," *The Astrophysical Journal*, vol. 727, no. 2, 2011.

[8] C. C. Porco, J. W. Weiss, D. C. Richardson, L. Dones, T. Quinn, and H. Throop, "Simulations of the dynamical and light-scattering behavior of saturn's rings and the derivation of ring particle and disk properties," *The Astronomical Journal*, vol. 136, no. 5, 2008.

[9] F. Ferrari, A. Tasora, P. Masarati, and M. Lavagna, "N-body gravitational and contact dynamics for asteroid aggregation," *Multibody System Dynamics*, vol. 39, pp. 3–20, 2017.

[10] F. Ferrari, M. Lavagna, and E. Blazquez, "A parallel-GPU code for asteroid aggregation problems with angular particles," *Monthly Notices of the Royal Astronomical Society*, vol. 492, no. 1, pp. 749–761, 2020.

[11] A. Tasora *et al.*, "Chrono: An open source multi-physics dynamics engine," in *High Performance Computing in Science and Engineering: Second International Conference, HPCSE 2015, Soláň, Czech Republic, May 25-28, 2015, Revised Selected Papers 2*, Springer, 2016, pp. 19–49.

[12] M. C. Nolan *et al.*, "Shape model and surface properties of the osiris-rex target asteroid (101955) bennu from radar and lightcurve observations," *Icarus*, vol. 226, no. 1, pp. 629–640, 2013.

[13] J. Fleischmann, R. Serban, D. Negrut, and P. Jayakumar, "On the importance of displacement history in soft-body contact models," *Journal of Computational and Nonlinear Dynamics*, vol. 11, no. 4, p. 044 502, 2016.

[14] M. Anitescu and A. Tasora, "An iterative approach for cone complementarity problems for nonsmooth dynamics," *Computational Optimization and Applications*, vol. 47, pp. 207–235, 2010.

[15] A. Tasora, M. Anitescu, S. Negrini, and D. Negrut, "A compliant visco-plastic particle contact model based on differential variational inequalities," *International Journal of Non-Linear Mechanics*, vol. 53, pp. 2–12, 2013.

[16] D. J. Scheeres, C. M. Hartzell, P. Sánchez, and M. Swift, "Scaling forces to asteroid surfaces: The role of cohesion," *Icarus*, vol. 210, no. 2, pp. 968–984, 2010.

[17] *Bremen drop tower payload user's guide, v. 1.3, 2019*.

[18] F. Gautier, E. Sitepu, C. Le Blay, G. Kersey, and J. Sánchez, "Drop your thesis! 2018 results: 4.74 seconds of microgravity conditions to enable future cubesat landings on asteroids," *Acta Astronautica*, vol. 176, pp. 139–155, 2020.

[19] B. Tweddle, A. Saenz-Otero, J. Leonard, and D. Miller, "Factor graph modeling of rigid-body dynamics for localization, mapping, and parameter estimation of a spinning object in space," *Journal of Field Robotics*, vol. 32, no. 6, pp. 897–933, 2015.

[20] F. Ornati, G. Di Domenico, P. Panicucci, and F. Topputo, "High-accuracy vision-based attitude estimation system for air-bearing spacecraft simulators," *arXiv*, 2023.

[21] P. A. Bland, G. Cressey, and O. N. Menzies, "Modal mineralogy of carbonaceous chondrites by X-ray diffraction and Mössbauer spectroscopy," *Meteoritics & Planetary Science*, vol. 39, no. 1, pp. 3–16, 2004.

[22] R. Hartley and A. I. Zisserman, *Multiple View Geometry in Computer Vision*. Cambridge University Press, 2004.

[23] Z. Zhang, "A flexible new technique for camera calibration," *IEEE Transactions on Pattern Analysis and Machine Intelligence*, vol. 22, no. 11, pp. 1330–1334, 2000.